Temperature-induced changes in the properties of the progenitor of the neutron star PSR J0952-0607*

Cheng-Jian Nie (聂承剑)[1] Xian-Feng Zhao (赵先锋)[2†]

[1]School of Intelligent Connected and New Energy Vehicles, Geely University of China, Chengdu 641423, China
[2]School of Sciences, Southwest Petroleum University, Chengdu 610500, China

Abstract: The temperature dependence of the properties of the progenitor of the neutron star PSR J0952-0607 is investigated within the relativistic mean-field theory using the NL1 nucleon coupling parameter set, with temperatures ranging from 10 to 35 MeV. The maximum mass exhibits a non-monotonic behavior: it decreases from 2.7502 $M_{\odot}$ at 10 MeV to 2.7445 $M_{\odot}$ at 25 MeV, then increases slightly to 2.7475 $M_{\odot}$ at 35 MeV. The corresponding radius at maximum mass expands monotonically from 13.66 to 15.81 km due to thermal pressure. As temperature rises, the central baryon density drops from 0.389 to 0.362 fm^{-3}, and the central neutron (electron) chemical potential decreases from 1312 (202) to 1232 (180) MeV. The relative density of neutrons decreases from 84.1% to 78.8%, while the proton fraction increases from 15.6% to 17.3%. Hyperons, especially Λ, appear and grow in abundance (from 0.3% to 2.7%), softening the EoS. These temperature-induced changes in composition and thermodynamics explain the observed non-monotonic variation of the maximum mass and the overall expansion of the star. This work provides essential insights into the early evolution of hot neutron stars.

Keywords: baryon, the relativistic mean field theory, proto neutron star

DOI: 10.1088/1674-1137/ae8ace **CSTR:** 32044.14.ChinesePhysicsC.50104109

I. INTRODUCTION

Neutron stars (NSs) are among the most compact observable objects in the universe and provide a natural laboratory for studying dense nuclear matter under extreme conditions [1−4]. Of particular interest are progenitors —hot, neutrino-trapped objects that form immediately after a core-collapse supernova, before cooling into cold NSs [5, 6]. During the early post-bounce phase, the temperature of a progenitor can reach several tens of MeV, and its properties are strongly influenced by thermal effects, trapped neutrinos, and the possible appearance of hyperons and other exotic degrees of freedom [7].

The equation of state (EOS) of dense matter is the key input for modeling progenitors. Within the relativistic mean-field (RMF) approach [8], various nucleon coupling parameter sets have been developed to reproduce empirical nuclear matter properties and astrophysical observations [9].

The discovery of several massive NSs in recent years represents a major advance in NS research. PSR J1614-2230 was measured to have $M = 1.93 \pm 0.07\ M_{\odot}$ [10, 11], followed by PSR J0348+0432 ($M = 2.01 \pm 0.04\ M_{\odot}$) in 2013 [12]. PSR J0740+6620 was first reported with $M = 2.14^{+0.10}_{-0.09}\ M_{\odot}$ in 2020 [13] and later revised to $M = 2.08 \pm 0.07\ M_{\odot}$ [14]. Miller *et al.* determined its radius to be $R = 13.7^{+2.6}_{-1.5}$ km [15]. In 2022, PSR J0952-0607, with a mass of $M = 2.35^{+0.17}_{-0.17}\ M_{\odot}$, was discovered [16]. Radius measurements of PSR J0030+0451 by the NICER collaboration [17, 18] provide stringent tests for theoretical models. Although PSR J0952-0607 is observed as a cold NS, its progenitor was a hot, neutrino-trapped object shortly after birth. In this work, we investigate the temperature dependence of the properties of this progenitor phase.

Temperature plays a crucial role in the evolution of a progenitor. It not only modifies the EOS but also affects the chemical potentials, particle fractions, and overall structure of the star [6]. Several studies have investigated the temperature dependence of progenitor properties [19, 20], but systematic explorations of the non-monotonic behavior of the maximum mass and the associated changes in central density, chemical potentials, and hyperon abundances remain limited, especially for the specific source PSR J0952-0607.

The discovery of massive NSs such as PSR J0952-0607 ($M = 2.35 \pm 0.11\ M_{\odot}$) provides a stringent test for

Received 25 May 2026; Accepted 15 July 2026; Accepted manuscript online 16 July 2026
* Supported by the Nationa Natural Science Foundation of China (12465023)
† E-mail: zhaopioneer.student@sina.com

the EOS of dense matter. While this pulsar is observed as a cold NS, it was born as a hot progenitor with temperatures of several tens of MeV. Understanding the temperature dependence of its progenitor properties is essential for reconstructing its birth conditions and for linking the hot, neutrino-trapped phase to the cold, observable remnant. In this work, we therefore systematically study the effects of temperature (10–35 MeV) on the maximum mass, radius, central thermodynamics, and baryon composition of the progenitor of the neutron star PSR J0952-0607 using the NL1 nucleon coupling parameter set within an RMF model that includes hyperons.

II. RELATIVISTIC MEAN-FIELD THEORY FOR PROGENITOR MATTER

The Lagrangian density for hadronic matter containing the mesons σ^* and ϕ is given by [7].

$$\begin{aligned}\mathcal{L}=&\sum_B\overline{\Psi}_B\left(\mathrm{i}\gamma_\mu\partial^\mu-m_B+g_{\sigma B}\sigma+g_{\sigma^*B}\sigma^*-g_{\omega B}\gamma^0\omega-g_{\phi B}\gamma^0\phi\right.\\&\left.-g_{\rho B}\gamma^0\tau_3\rho\right)\Psi_B-\frac{1}{2}m_\sigma^2\sigma^2-\frac{1}{3}g_2\sigma^3-\frac{1}{4}g_3\sigma^4+\frac{1}{2}m_\omega^2\omega^2\\&+\frac{1}{2}m_\rho^2\rho^2-\frac{1}{2}m_{\sigma^*}^2\sigma^{*2}+\frac{1}{2}m_\phi^2\phi^2+\sum_{\lambda=e,\mu}\overline{\Psi}_\lambda\left(\mathrm{i}\gamma_\mu\partial^\mu-m_\lambda\right)\Psi_\lambda.\end{aligned} \tag{1}$$

Mesons $f_0(975)$ (denoted as σ^*) and $\phi(1020)$ (denoted as ϕ) mediate the interactions between nucleons and hyperons [21].

Considering neutrino trapping, the baryon partition function of the progenitor matter is [22, 23]

$$\ln Z_B=\frac{V}{T}\langle\mathcal{L}\rangle+\sum_B\frac{2J_B+1}{2\pi^2}\int_0^\infty k^2\mathrm{d}k\left\{\ln\left[1+\mathrm{e}^{-(\varepsilon_B(k)-\mu_B)/T}\right]\right\}. \tag{2}$$

Thus, the total baryon number density is obtained as follows:

$$\rho=\sum_B\frac{2J_B+1}{2\pi^2}b_B\int_0^\infty k^2n_B(k)\mathrm{d}k. \tag{3}$$

The energy density and pressure, respectively, are

$$\begin{aligned}\varepsilon=&\frac{1}{2}m_\sigma^2\sigma^2+\frac{1}{2}m_{\sigma^*}^2\sigma^{*2}+\frac{1}{3}g_2\sigma^3+\frac{1}{4}g_3\sigma^4\\&+\frac{1}{2}m_\omega^2\omega_0^2+\frac{1}{2}m_\phi^2\phi^2+\frac{1}{2}m_\rho^2\rho_{03}^2\\&+\sum_B\frac{2J_B+1}{2\pi^2}\int_0^\infty k^2n_B(k)\mathrm{d}k\sqrt{k^2+m_B^{*2}},\end{aligned} \tag{4}$$

$$\begin{aligned}p=&-\frac{1}{2}m_\sigma^2\sigma^2-\frac{1}{2}m_{\sigma^*}^2\sigma^{*2}-\frac{1}{3}g_2\sigma^3-\frac{1}{4}g_3\sigma^4\\&+\frac{1}{2}m_\omega^2\omega_0^2+\frac{1}{2}m_\phi^2\phi^2+\frac{1}{2}m_\rho^2\rho_{03}^2\\&+\frac{1}{3}\sum_B\frac{2J_B+1}{2\pi^2}\int_0^\infty\frac{k^4}{\sqrt{k^2+m_B^{*2}}}n_B(k)\mathrm{d}k.\end{aligned} \tag{5}$$

Here, $n_B(k)$ is the Fermi-Dirac partition function for baryons.

$$n_B(k)=\frac{1}{1+\exp\left[(\varepsilon_B(k)-\mu_B)/T\right]}, \tag{6}$$

and m_B^* is the effective mass of the baryons.

$$m_B^*=m_B-g_{\sigma B}\sigma-g_{\sigma^*B}\sigma^*. \tag{7}$$

In this work, the mean-field values of the meson fields σ, ω, ρ, σ^*, and ϕ are determined self-consistently at each temperature T by solving the finite-temperature equations of motion, rather than the $T=0$ field equations. For the σ field, the equation reads

$$m_\sigma^2\sigma+g_2\sigma^2+g_3\sigma^3=\sum_B g_{\sigma B}\rho_S^{(B)}, \tag{8}$$

where the scalar density

$$\rho_S^{(B)}=\frac{2J_B+1}{2\pi^2}\int k^2\mathrm{d}k\frac{m_B^*}{\sqrt{k^2+m_B^{*2}}}n_B(k). \tag{9}$$

It is computed using the finite-temperature Fermi-Dirac distribution $n_B(k)$ (Eq. (6)). Similarly, the source terms in the ω, ρ, σ^* and ϕ field equations are also obtained from $n_B(k)$. For a given T and total baryon density ρ, the meson fields are solved iteratively until convergence is reached. Consequently, the meson fields evolve with temperature and are not fixed at their $T=0$ values.

Neglecting lepton interactions at finite temperature, we write their partition function as

$$\begin{aligned}\ln Z_L=&\frac{V}{T}\sum_i\frac{\mu_i^4}{24\pi^2}\left[1+2\left(\frac{\pi T}{\mu_i}\right)^2+\frac{7}{15}\left(\frac{\pi T}{\mu_i}\right)^4\right]\\&+V\sum_\lambda\frac{1}{\pi^2}\int_0^\infty k^2\mathrm{d}k\left\{\ln\left[1+\mathrm{e}^{-(\varepsilon_\lambda(k)-\mu_\lambda)/T}\right]\right\}.\end{aligned} \tag{10}$$

The first line represents the contribution from massless neutrinos, and the second line represents the contribution from electrons and μs.

The lepton number density is

$$\rho_l = \frac{1}{\pi^2}\int_0^\infty k^2 n_l(k)\mathrm{d}k, \tag{11}$$

$$\rho_\nu = \frac{\pi^2 T^2 \mu_\nu + \mu_\nu^3}{6\pi^2}, \tag{12}$$

and the contributions of leptons to the energy density and pressure are

$$\varepsilon = \sum_l \frac{1}{\pi^2}\int_0^\infty k^2 n_l(k)\mathrm{d}k\sqrt{k^2+m_l^2} + \sum_\nu\left(\frac{7\pi^2 T^4}{120} + \frac{T^2\mu_\nu^2}{4} + \frac{\mu_\nu^4}{8\pi^2}\right), \tag{13}$$

$$p = \frac{1}{3}\sum_l \frac{1}{\pi^2}\int_0^\infty \frac{k^4}{\sqrt{k^2+m_l^2}} n_l(k)\mathrm{d}k + \sum_\nu \frac{1}{360}\left(7\pi^2 T^4 + 30T^2\mu_\nu^2 + \frac{15\mu_\nu^4}{\pi^2}\right). \tag{14}$$

In this work, we assume that neutrinos have already escaped; that is, the neutrino chemical potential is set to zero ($\mu_\nu = 0$). Therefore, the electron fraction is determined self-consistently from charge neutrality and beta equilibrium, without prescribing any lepton fraction. This approximation is valid during the later stages of progenitor evolution (the neutrino-transparent phase). Studies of the early trapped stage, with a fixed lepton fraction, will be pursued in future work.

We can calculate the mass and radius of a progenitor using the Tolman-Oppenheimer-Volkoff (TOV) equation [24, 25].

$$\frac{\mathrm{d}p}{\mathrm{d}r} = -\frac{(p+\varepsilon)\left(M+4\pi r^3 p\right)}{r(r-2M)}, \tag{15}$$

$$M = 4\pi\int_0^R \varepsilon r^2 \mathrm{d}r. \tag{16}$$

III. PARAMETERS

We employ seven sets of nucleon coupling parameters to describe the EoS of the progenitor: NL1 [26], FSUGold [27], FSU2R [28], FSU2H [28], GL85 [9], GL97 [7], and GM1 [29]. First, we select one of these seven nucleon coupling parameter sets to describe the progenitor of the neutron star PSR J0952-0607. At this stage, the temperature of the progenitor is taken to be T = 15 MeV.

The ratios of hyperon coupling constants to nucleon coupling constants are defined as $x_{\sigma h} = g_{\sigma h}/g_\sigma$, $x_{\omega h} = g_{\omega h}/g_\omega$, and $x_{\rho h} = g_{\rho h}/g_\rho$, where h denotes the hyperons Λ, Σ, and Ξ. These ratios typically lie in the range ~ 1/3 to 1 [29]. The values of $x_{\rho h}$ are chosen according to quark SU(6) symmetry [30, 31]. To obtain a sufficiently large progenitor mass, we set $x_{\omega h} = 0.9$, while $x_{\sigma h}$ is determined by the following relation [7]:

$$U_h^{(N)} = m_n\left(\frac{m_n^*}{m_n} - 1\right)x_{\sigma h} + \left(\frac{g_\omega}{m_\omega}\right)^2 \rho_0 x_{\omega h}. \tag{17}$$

The hyperon potentials are taken to be $U_\Lambda^{(N)} = -30$ MeV [31−33], $U_\Sigma^{(N)} = 30$ MeV [31−34], and $U_\Xi^{(N)} = -20$ MeV [35]. The interactions among hyperons are described by the coupling parameters of the σ^* and ϕ mesons to hyperons [21]:

$$g_{\phi\Xi} = 2g_{\phi\Lambda} = 2g_{\phi\Sigma} = -\frac{2\sqrt{2}}{3}g_\omega, \tag{18}$$

$$g_{\sigma^*\Lambda}/g_\sigma = g_{\sigma^*\Sigma}/g_\sigma = 0.69, \tag{19}$$

$$g_{\sigma^*\Xi}/g_\sigma = 1.25. \tag{20}$$

Figure 1 shows the mass-radius (M-R) relations calculated with the seven nucleon coupling parameter sets. The progenitor temperature is set to T = 15 MeV. The observational constraints from Riley *et al.* [17] (horizontally hatched region) and Miller *et al.* [18] (vertically hatched region) are also plotted for reference. Among all parameter sets, NL1 (highlighted as a thick curve) yields a maximum mass (~ $2.8M_\odot$) that comfortably exceeds the mass of PSR J0952-0607 (2.35 $M_\odot$), while most other sets produce significantly lower maximum masses. Moreover, the radii predicted by NL1 for masses around $1.4M_\odot$ are consistent with the measurements of Riley *et al.* and Miller *et al.*, which correspond to PSR J0030+0451. Therefore, the NL1 parameter set is selected for the subsequent investigation of temperature effects on the properties of the progenitor of the neutron star PSR J0952-0607. The progenitor temperatures are taken as $T = 10, 15, 20, 25, 30$, and 35 MeV, respectively.

IV. EFFECTS OF T ON $M_{\max}$, RADIUS, AND CENTRAL THERMODYNAMICS

As shown in Fig. 2, the mass-radius ($M-R$) relations of the progenitor of the neutron star PSR J0952-0607 exhibit a clear temperature dependence. With increasing temperature, the radius at a given mass (2.35 $M_\odot$) increases monotonically, reflecting the enhancement of thermal pressure. The corresponding maximum mass

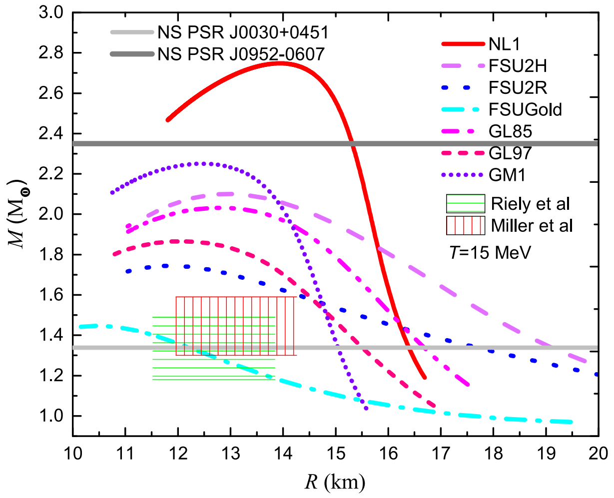

Fig. 1. (color online) Mass-radius relations for progenitors calculated with the seven nucleon coupling parameter sets considered in this work: FSUGold, FSU2R, FSU2H, GL85, GL97, GM1, and NL1. The NL1 result is shown as a thick solid curve and is selected for the present study because it satisfies the mass constraint of NS PSR J0952-0607 (horizontal gray band). The curves obtained with the other parameter sets are shown as thin curves in the figure. The thick horizontal line in light gray indicates the mass of the NS PSR J0030+0451, and the observational constraints on the mass of this star are shown as a shaded box (horizontal line: Riley *et al.*; vertical line: Miller *et al.*).

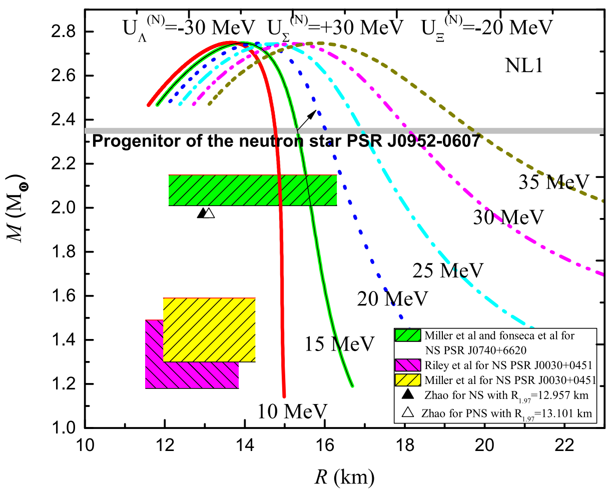

Fig. 2. (color online) Mass-radius (M-R) relations of the progenitor of the neutron star PSR J0952-0607 at different temperatures (T = 10−35 MeV) using the NL1 nucleon coupling parameter set. The temperature increases from the red to the dark-yellow curves. The maximum of each curve corresponds to the maximum mass of the progenitor at that temperature.

$M_{\max}$, whose corresponding radius is denoted as R_m, the central energy density as $\varepsilon_{c,m}$, and the central pressure as $p_{c,m}$, however, varies non-monotonically with temperature (Fig. 3 and Table 1). Between 10 and 25 MeV, $M_{\max}$ decreases gradually, whereas from 25 to 35 MeV it increases slightly.

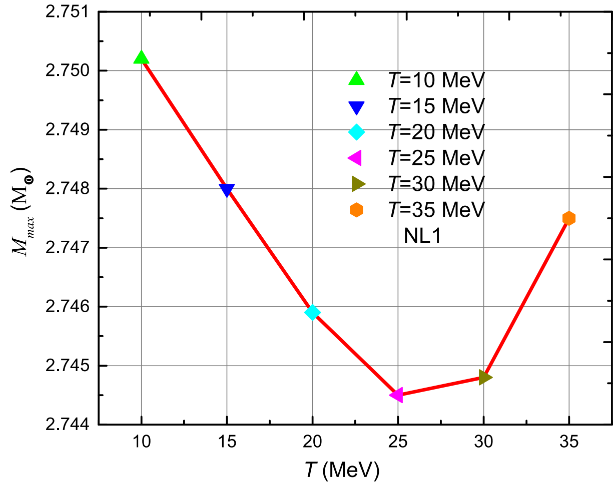

Fig. 3. (color online) Maximum progenitor mass $M_{\max}$ as a function of temperature T. Non-monotonic behavior is observed: $M_{\max}$ decreases from 10 MeV to 25 MeV and then increases from 25 MeV to 35 MeV.

Table 1. Maximum mass $M_{\max}$, corresponding radius R_m, central energy density $\varepsilon_{c,m}$, and central pressure $p_{c,m}$ of the progenitors at different temperatures T using the NL1 nucleon coupling parameter set.

T/MeV	$M_{\max}/M_\odot$	R_m/km	$\varepsilon_{c,m}\times10^{15}$ g·cm^{-3}	$p_{c,m}\times10^{35}$ dyne·cm^{-2}
10	2.750	13.65	1.468	5.817
15	2.748	13.94	1.471	5.833
20	2.746	14.29	1.469	5.817
25	2.745	14.71	1.466	5.786
30	2.745	15.21	1.459	5.723
35	2.748	15.81	1.442	5.596

This behavior can be understood by examining the central energy density $\varepsilon_{c,m}$ and central pressure $p_{c,m}$ at the maximum-mass configuration (Fig. 4). When the temperature increases from 10 to 15 MeV, both $\varepsilon_{c,m}$ and $p_{c,m}$ increase. Although this stiffens the core, the concurrent appearance of thermal excitations (*e.g.*, hyperons) softens the overall EOS, leading to a net decrease in $M_{\max}$. Between 15 and 35 MeV, $\varepsilon_{c,m}$ and $p_{c,m}$ decrease monotonically. The reduction in central density lowers the gravitational binding, while the thermal pressure continues to rise, eventually causing a mild increase in $M_{\max}$ above 25 MeV. The underlying EOS (Fig. 5) shows that, for a given energy density, the pressure decreases with temperature. This alone would not cause expansion; rather, the radial expansion seen in Fig. 2 results from thermal expansion: higher temperatures generate additional thermal pressure at a given density, which lowers the central density and enlarges the star.

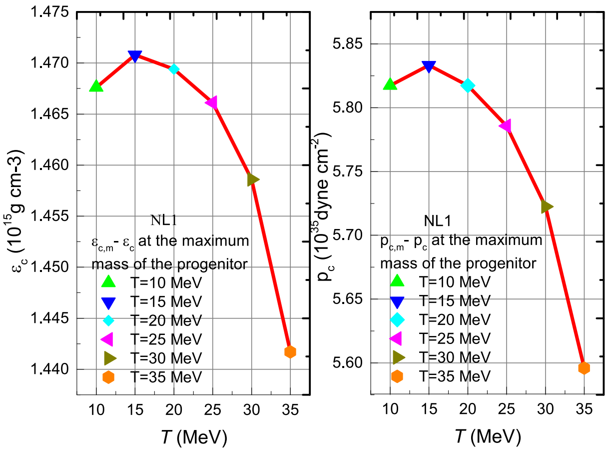

Fig. 4. (color online) (a) Central energy density $\varepsilon_{c,m}$ and (b) central pressure $p_{c,m}$ of the progenitor at the maximum-mass configuration as functions of temperature *T*. Both quantities exhibit a peak around 15 MeV, which explains the turning point of $M_{\max}$ in Fig. 3.

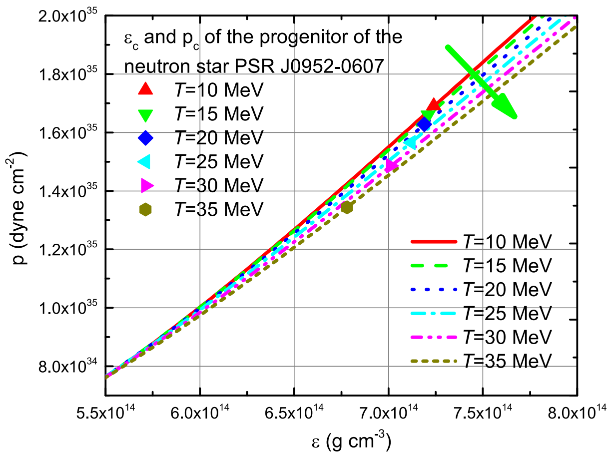

Fig. 5. (color online) EOS (pressure *p* versus energy density *ε*) of the progenitor at different temperatures. The thermal pressure increases with temperature at a fixed energy density, leading to the expansion of the star (increase in radius) shown in Fig. 2.

Thus, the interplay between thermal pressure, central density, and particle composition (see Fig. 8) gives rise to the observed nonlinear response of the maximum mass to temperature in this progenitor.

The increase in $M_{\max}$ above 25 MeV, which appears to contradict the decreasing central pressure, can be understood as the result of competition between hyperon-induced softening and thermal-pressure hardening. Between 10 and 25 MeV, thermal excitation triggers the appearance of hyperons (mainly Λ, Σ^-, and Ξ^-), softening the EoS and reducing $M_{\max}$. When the temperature exceeds 25 MeV, hyperon abundances tend to saturate, while the thermal pressure (scaling as T^2 or T^4) continues to grow nonlinearly. This thermal contribution partially compensates for the pressure loss associated with the decreasing central density, and the lower central density also suppresses further hyperon production. Consequently, the net stiffness of the EOS slightly increases above 25 MeV, leading to a mild recovery of $M_{\max}$. Thus, 25 MeV can be identified as the transition temperature at which the dominant effect switches from hyperon softening to thermal-pressure hardening.

To ensure the reliability of the TOV solutions, we performed convergence tests. Halving the radial integration step size from 0.001 to 0.0005 km left the maximum mass unchanged (variation < 10^{-5} $M_\odot$) for all temperatures, with radius changes below 0.01 km. Reducing the central-pressure scan step from 0.005 to 0.0025 fm^{-4} also produced no change in the maximum mass; the tiny radius variations (⩽0.02 km) are physically negligible. Hence, the step sizes used in this work ensure numerical convergence. The observed temperature variation of the maximum mass (0.0057 $M_\odot$) is an order of magnitude larger than the numerical uncertainty (<0.0005 $M_\odot$), confirming its physical significance.

V. TEMPERATURE DEPENDENCE OF CENTRAL ρ_c, $\mu_{n,c}$, AND $\mu_{e,c}$

Figure 6 shows the variation in the central baryon density ρ_c of the progenitor of the neutron star PSR J0952-0607 as a function of temperature *T*, calculated using the NL1 nucleon coupling parameter set. The corresponding numerical values are listed in Table 2.

As shown in Fig. 6, ρ_c decreases monotonically with increasing temperature *T*. When the temperature rises from 10 to 35 MeV, the central density drops from 0.389 to 0.362 fm^{-3}. This monotonic decline is a direct consequence of thermal expansion: higher temperatures generate additional thermal pressure, which causes the star to expand and, for a given stellar mass, reduces the central density. The decrease is relatively slow between 10 and 20 MeV (from 0.389 to 0.385 fm^{-3}), becomes slightly steeper between 20 and 30 MeV (down to 0.374 fm^{-3}), and then accelerates above 30 MeV, reaching 0.362 fm^{-3} at 35 MeV. This behavior suggests that thermal pressure becomes increasingly effective at higher temperatures, leading to more rapid core expansion.

The reduction in ρ_c with temperature is consistent with the observed softening of the EOS and the decrease in maximum mass (see Fig. 3 and Table 1). A lower central density implies a lower Fermi energy for neutrons and electrons, which directly explains the accompanying decrease in the central chemical potentials $\mu_{n,c}$ and $\mu_{e,c}$ listed in Table 2. The nearly linear, but accelerating, de-

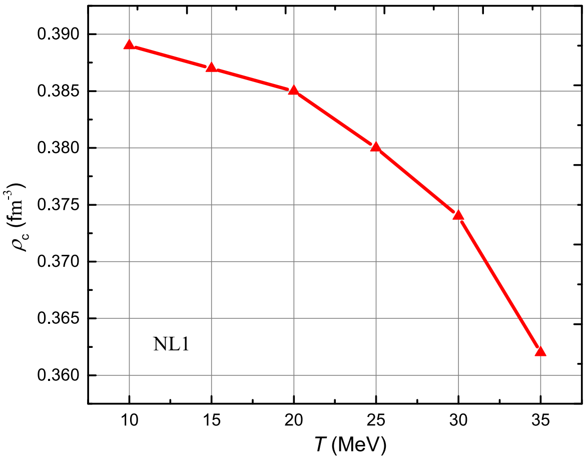

Fig. 6. (color online) The central baryon density ρ_c of the progenitor of the neutron star PSR J0952-0607 as a function of temperature T, obtained using the NL1 nucleon coupling parameter set.

Table 2. Central baryon density ρ_c, central neutron chemical potential $\mu_{n,c}$, and central electron chemical potential $\mu_{e,c}$ of the progenitor of the neutron star PSR J0952-0607 at different temperatures T, calculated using the NL1 nucleon coupling parameter set.

T/MeV	ρ_c/fm^{-3}	$\mu_{n,c}$/MeV	$\mu_{e,c}$/MeV
10	0.389	1312.01	202.14
15	0.387	1304.62	199.89
20	0.385	1296.02	196.72
25	0.380	1280.29	192.16
30	0.374	1261.97	186.77
35	0.362	1231.56	179.79

cline of ρ_c with T indicates that thermal effects on the core structure are not negligible, especially in the high-temperature regime ($T \geqslant 30$ MeV).

In summary, Fig. 6 together with Table 2 clearly demonstrates that temperature plays a significant role in determining the central compression of the progenitor. The monotonic decrease of ρ_c with rising temperature is a key feature that underpins many of the temperature-dependent properties discussed in this work, including the reduction in maximum mass and the associated changes in central chemical potentials.

Figure 7 (left panel) displays the central neutron chemical potential $\mu_{n,c}$ as a function of the central baryon density ρ_c for the progenitor of the neutron star PSR J0952-0607 at six different temperatures, while the right panel shows the corresponding central electron chemical potential $\mu_{e,c}$. The numerical values are summarized in Table 2.

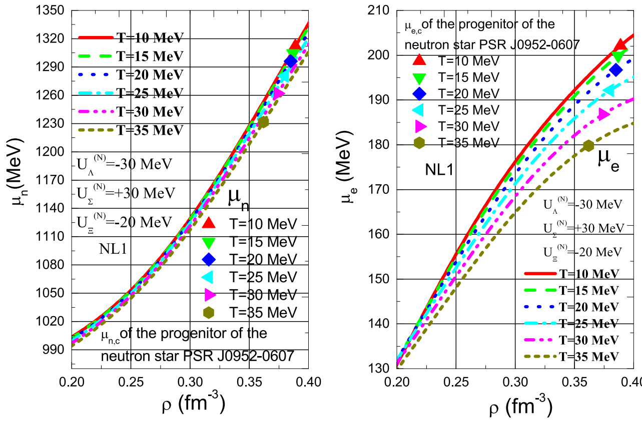

Fig. 7. (color online) Neutron chemical potential μ_n (left panel) and electron chemical potential μ_e (right panel) as functions of baryon number density ρ for the progenitor of the neutron star PSR J0952-0607 at temperatures $T = 10$, 15, 20, 25, 30, and 35 MeV, calculated using the NL1 nucleon coupling parameter set.

Both $\mu_{n,c}$ and $\mu_{e,c}$ decrease monotonically as ρ_c decreases with increasing temperature T. When the temperature T rises from 10 to 35 MeV, ρ_c drops from 0.389 to 0.362 fm^{-3}. Concurrently, $\mu_{n,c}$ decreases from 1312.01 to 1231.56 MeV, and $\mu_{e,c}$ decreases from 202.14 to 179.79 MeV. This behavior reflects the thermal expansion of the star: higher temperatures generate additional thermal pressure, which lowers the central density and, consequently, reduces the Fermi energies (and thus the chemical potentials) of both neutrons and electrons.

The decrease is not strictly linear. Between 10 and 25 MeV, the reductions in ρ_c, $\mu_{n,c}$, and $\mu_{e,c}$ are relatively gradual. Above 30 MeV, the decline becomes more pronounced, especially for $\mu_{n,c}$, which drops by about 30 MeV from 30 to 35 MeV. This accelerated decrease at higher temperatures suggests that thermal pressure becomes increasingly effective in expanding the core, thereby reducing the density and degeneracy more rapidly.

Throughout the entire temperature range, $\mu_{n,c}$ remains much larger than $\mu_{e,c}$, consistent with beta equilibrium and charge neutrality in dense neutron-rich matter. The monotonic decrease of both chemical potentials with rising temperature, and hence with falling ρ_c, is a direct consequence of the thermal softening of the EOS and the associated reduction in central compression.

In summary, Fig. 7 and Table 2 together demonstrate that the central chemical potentials of the progenitor are strongly correlated with the central density, which itself decreases with temperature T. The temperature-induced drop in $\mu_{n,c}$ and $\mu_{e,c}$ is consistent with the overall thermal expansion and the reduction in maximum mass observed at higher temperatures (see Fig. 3 and Table 1).

VI. TEMPERATURE DEPENDENCE OF BARYON FRACTIONS IN THE PROGENITOR OF THE NEUTRON STAR PSR J0952-0607

Figure 8 shows the evolution of the relative baryon number densities in the progenitor of the neutron star PSR J0952-0607 as temperature increases, while Table 3 lists the numerical values at the stellar center. Several clear trends emerge.

As the temperature rises from 10 to 35 MeV, the central relative neutron density decreases monotonically from about 84.1% to 78.8% (see Table 3, column $\rho_{n,c}/\rho$). This decrease is compensated by increases in the relative densities of protons and hyperons. The proton fraction rises from 15.6% to 17.3%, consistent with a shift toward more symmetric nuclear matter at higher temperatures due to the thermal excitation of protons. Among the hyperons, the Λ fraction increases steadily from 0.3% to 2.7%, becoming the most abundant hyperon at all temperatures. The Σ^- fraction, though very small at low T (2.8×10^{-4}% at 10 MeV), increases to 0.4% at 35 MeV. Similarly, the Ξ^- fraction rises from 9.4×10^{-3}% to 0.8% over the same temperature range. The Σ^+ and Σ^0 fractions remain extremely low (≤ 0.02%) even at the highest temperature, while Ξ^0 appears only above 20 MeV and reaches 0.01% at 35 MeV.

The progressive conversion of neutrons into protons and hyperons with increasing temperature is a direct consequence of thermal activation: higher temperatures allow more massive strange baryons to be populated via strong and weak interactions, thereby softening the EoS and influencing global stellar properties such as the maximum mass and radius. The central baryon density ρ_c simultaneously decreases, from 0.389 to 0.362 fm^{-3} (see Table 3), indicating that thermal expansion accompanies the compositional changes. Thus, Fig. 8 and Table 3 together demonstrate that temperature plays a crucial role in reshaping the internal baryonic composition of a hot

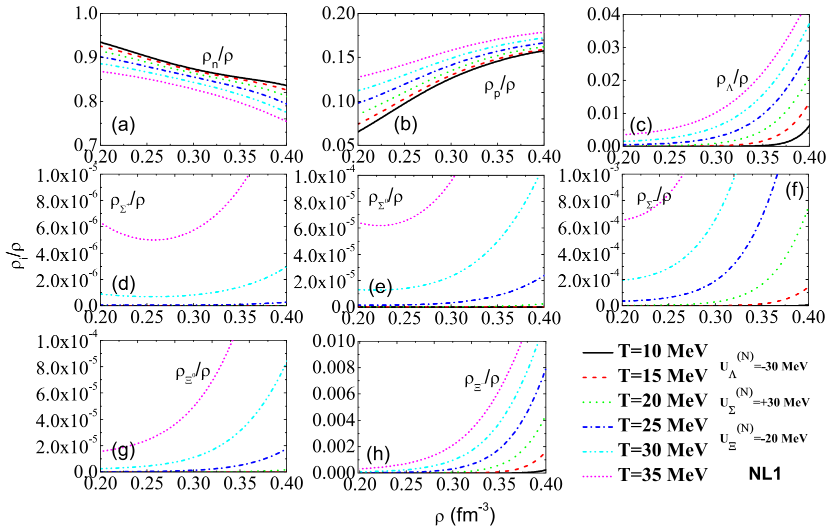

Fig. 8. (color online) Temperature dependence of the relative number densities of baryons in the progenitor of the neutron star PSR J0952-0607. Panels (a)–(h) show the relative number densities of neutrons, protons, and hyperons (Λ, Σ^+, Σ^0, Σ^-, Ξ^0, and Ξ^-) as functions of temperature T (10−35 MeV), calculated with the NL1 nucleon coupling parameter set. The central relative number densities at each temperature are listed in Table 3.

Table 3. Central relative particle densities (in percentage) of neutrons, protons, and hyperons (Λ, Σ^+, Σ^0, Σ^-, Ξ^0, and Ξ^-) in the progenitor of the neutron star PSR J0952-0607 at temperatures T ranging from 10 to 35 MeV, calculated with the NL1 nucleon coupling parameter set. The central baryon density ρ_c (in fm^{-3}) is also listed for each temperature.

T/MeV	ρ_c/fm^{-3}	$\rho_{n,c}/\rho$/%	$\rho_{p,c}/\rho$/%	$\rho_{\Lambda,c}/\rho$/%	$\rho_{\Sigma^+,c}/\rho$/%	$\rho_{\Sigma^0,c}/\rho$/%	$\rho_{\Sigma^-,c}/\rho$/%	$\rho_{\Xi^0,c}/\rho$/%	$\rho_{\Xi^-,c}/\rho$/%
10	0.389	84.1	15.6	0.3	0	0	2.8×10^{-4}	0	9.4×10^{-3}
15	0.387	83.4	15.7	0.8	0	4×10^{-6}	8.4×10^{-6}	2.0×10^{-6}	0.08
20	0.385	82.3	16.0	1.4	1.0×10^{-6}	1.8×10^{-4}	0.05	1.1×10^{-4}	0.3
25	0.380	81.1	16.3	1.9	2×10^{-5}	1.6×10^{-3}	0.1	1.1×10^{-3}	0.5
30	0.374	79.8	16.8	2.4	2.0×10^{-4}	7.3×10^{-3}	0.3	5.1×10^{-3}	0.7
35	0.362	78.8	17.3	2.7	1.0×10^{-3}	0.02	0.4	0.01	0.8

progenitor.

VII. SUMMARY

The effects of temperature (10−35 MeV) on the properties of the progenitor of the neutron star PSR J0952-0607 were systematically investigated using the NL1 nucleon coupling parameter set within an RMF model that includes hyperon degrees of freedom. The main findings are as follows.

The maximum mass decreases slightly from 2.7502 $M_\odot$ at 10 MeV to 2.745 $M_\odot$ at 25 MeV, then increases marginally to 2.748 $M_\odot$ at 35 MeV, exhibiting non-monotonic behavior. The corresponding radius at maximum mass increases monotonically from 13.66 to 15.81 km, reflecting thermal expansion.

At a fixed energy density, the pressure increases with temperature, indicating thermal stiffening. However, due to the accompanying decrease in central density, the central pressure itself decreases at higher temperatures.

The central baryon density ρ_c decreases from 0.389 to 0.362 fm^{-3} as T increases from 10 to 35 MeV. Consequently, the central neutron and electron chemical potentials $\mu_{n,c}$ and $\mu_{e,c}$ decrease from 1312 to 1232 MeV and from 202 to 180 MeV, respectively.

With increasing temperature, the central neutron relative density decreases (84.1% → 78.8%), while the proton fraction increases (15.6% → 17.3%). Hyperons (Λ, Σ^-, Ξ^-) appear and become more abundant, with Λ becoming the most abundant hyperon (0.3% → 2.7%). The onset of hyperons softens the EOS and contributes to the non-monotonic behavior of the maximum mass.

In summary, temperature significantly influences the global structure, EOS, central thermodynamics, and baryonic composition of the progenitor of the neutron star PSR J0952-0607. The interplay among thermal pressure, hyperon appearance, and density reduction leads to a complex, nonlinear response of the star's properties, which is essential for understanding the early cooling evolution and observable signatures of such objects.

References

[1] C. J. Xia, T. Maruyama, and N. Yasutake, Phys. Rev. D **110**, 114024 (2024)
[2] Z. L. Deng, Z. F. Gao, and X. D. Li, Astrophys. J. **892**, 4 (2020)
[3] W. B. Ding, M. D. Cai, and A. H. Chan, Int. J. Mod. Phys. A **37**, 2250034 (2022)
[4] X. L. Mu, H. Y. Jia, and X. Zhou, Astrophys. J. **846**, 140 (2017)
[5] A. Burrows and J. M. Lattier, Astrophys. J. **307**, 178 (1986)
[6] M. Prakash, I. Bombaci, Phys. Rep. **280**, 1 (1997)
[7] N. Glendenning, *Compact Stars: Nucl. Phys., Particle Physics, and General Relativity* (New York: Springer-Verlag, 1997)
[8] S. G. Zhou, Physica Scripta **91**, 063008 (2016)
[9] N. Glendenning, Astrophys. J. **293**, 470 (1985)
[10] P. B. Demorest, T. Pennucci, S. M. Ransom *et al.*, Nature **467**, 1081 (2010)
[11] E. Fonseca, T. T. Pennucci, J. A. Ellis *et al.*, Astrophys. J. **832**, 167 (2016)
[12] J. Antoniadis, P. C. C. Freire, Science **340**, 448 (2013)
[13] H. T. Cromartie, E. Fonseca, and S. M. Ransom, Nat. Astron. **4**, 72 (2020)
[14] E. Fonseca, C. E. T, P. T. T *et al.*, Astrophys. J. Lett. **915**, L12 (2021)
[15] M. C. Miller, F. K. Lamb, A. J. Dittmann *et al.*, Astrophys. J. Lett. **918**, L28 (2021)
[16] R. W. Romani, D. Kandel, A. V. Filippenko *et al.*, Astrophys. J. Lett. **934**, L17 (2022)
[17] T. E. Riley, A. L. Watts, S. Bogdanov *et al.*, Astrophys. J. Lett. **887**, L21 (2019)
[18] M. C. Miller, F. K. Lamb, A. J. Dittmann *et al.*, Astrophys. J. Lett. **887**, L24 (2019)
[19] O. Nicotra, M. Baldo, G. Burgio, and H. Schulze, Astron. Astrophys. **451**, 213 (2006)
[20] J. A. Pons, S. Reddy, M. Prakash *et al.*, Astrophys. J. **513**, 780 (1999)
[21] J. Schaffner, C. B. Dover, A. Gal *et al*, Ann. Phys. **235**, 35 (1994)
[22] N. Glendenning, Phys. Lett. B **185**, 275 (1987a)
[23] N. Glendenning, Nucl. Phys. A **469**, 600 (1987b)
[24] R. C. Tolman, Phys. Rev. **55**, 364 (1939)
[25] J. R. Oppenheimer and G. M. Volkoff, Phys. Rev. **55**, 374 (1939)
[26] S. J. Lee, J. Fink, and A. B. Balantekin, Phys. Rev. Lett. **57**, 2916 (1986)
[27] B. G. Todd-Rutel and J. Piekarewicz, Phys. Rev. Lett. **95**, 122501 (2005)
[28] L. Tolos, M. Centelles, and A. Ramos, Publ. Astron. Soc. Aust. **34**, e065 (2017)
[29] N. Glendenning and S. A. Moszkowski, Phys. Rev. Lett. **67**, 2414 (1991)
[30] J. Schaffner and I. N. Mishustin, Phys. Rev. C **53**, 1416 (1996)
[31] J. Schaffner-Bielich and A. Gal, Phys. Rev. C **62**, 034311 (2000)
[32] S. Weissenborn, D. Chatterjee, J. Schaffner-Bielich *et al.*, Phys. Rev. C **85**, 065802 (2012)
[33] A. Gal, E. V. Hungerford, and D. J. Millener, Rev. Mod. Phys. **88**, 035004 (2016)
[34] C. J. Batty, E. Friedman, and A. Gal, Phys. Rep. **287**, 385 (1997)
[35] T. Harada, Y. Hirabayashi, and A. Umeya, Phys. Lett. B **690**, 363 (2010)